Towards a Classification Model using CNN and Wavelets applied to COVID-19 CT images

Por um modelo de classificação usando CNN e Wavelets aplicados a imagens de TC COVID-19

Hacia un Modelo de Clasificación usando CNN y Wavelets aplicado a imágenes de TC de COVID-19

Pedro Moises de Sousa
ORCID: https://orcid.org/0000-0003-4563-0033
Federal University of Uberlândia, Brazil
E-mail: pedrosousa@ufu.br
Pedro Cunha Carneiro
ORCID: https://orcid.org/0000-0002-0120-5273
Federal University of Uberlândia, Brazil
E-mail: pedrocarneiro@ufu.br
Gabrielle Macedo Pereira
ORCID: https://orcid.org/0000-0002-1482-4946
Federal University of Uberlândia, Brazil
E-mail: gabriellemp@ufu.br
Mariane Modesto Oliveira
ORCID: https://orcid.org/0000-0003-4368-7087
Federal University of Uberlândia, Brazil
E-mail: modestomariane@gmail.com
Carlos Alberto da Costa Junior
ORCID: https://orcid.org/0000-0003-1915-9137
Federal University of Uberlândia, Brazil
E-mail: carlosjunior@ufu.br
Luis Vinicius de Moura
ORCID: https://orcid.org/0000-0003-3429-3289
Pontifical Catholic University of Rio Grande do Sul, Brazil
E-mail: luis.moura@edu.pucrs.br
Christian Mattjie
ORCID: https://orcid.org/0000-0002-3745-8686
Pontifical Catholic University of Rio Grande do Sul, Brazil
E-mail: christian.mattjie@gmail.com
Ana Maria Marques da Silva
ORCID: https://orcid.org/0000-0002-5924-6852
Pontifical Catholic University of Rio Grande do Sul, Brazil
E-mail: ana.marques@pucrs.br
Túlio Augusto Alves Macedo
ORCID: https://orcid.org/0000-0002-4029-2349
Federal University of Uberlândia, Brazil
E-mail: tuliomacedo@ufu.br
Ana Claudia Patrocinio
ORCID: https://orcid.org/0000-0001-9376-7689
Federal University of Uberlândia, Brazil
E-mail: ana.patrocinio@ufu.br

Abstract
In late 2019, a new type of coronavirus emerged in China and was named SARS-CoV-2. It first impacted the country where it emerged and then spread around the world. SARS-CoV-2 is the cause of COVID-19 disease that leaves characteristic impressions on chest CT images of infected patients. In this article, we propose a classification model, based on CNN and wavelet transform, to classify images of COVID-19 patients. It was named WCNN-COVID. The model was applied and tested in open and private TC image repositories. A total of 25534 images of 200 patients were processed. The confusion matrix was generated by calculating Accuracy (ACC), Sensitivity (Sen) and Specificity (Sp). The Receiver Operating Characteristic (ROC) curve and Area Under the Curve (AUCs) were also plotted and used for evaluation. Metric results were ACC = 0.9950, Sen = 99.16% and Sp = 99.89%.
Keywords: CT images; Convolutional Neural Networks; COVID-19; Wavelets; WCN-COVID.

Resumo

No final de 2019, um novo tipo de coronavírus surgiu na China e recebeu o nome de SARS-CoV-2. Primeiro impactou o país onde surgiu e depois se espalhou pelo mundo. O SARS-CoV-2 é a causa da doença COVID-19 que deixa impressões características nas imagens de TC de tórax dos pacientes infectados. Neste artigo, propomos um modelo de classificação, baseado em CNN e transformada wavelet, para classificar imagens de pacientes COVID-19. Ele foi denominado WCNN-COVID. O modelo foi aplicado e testado em repositórios de imagens de TC abertos e privados. Foram processadas 25534 imagens de 200 pacientes. A matriz de confusão foi gerada pelo cálculo de Acurácia (ACC), Sensibilidade (Sen) e Especificidade (Sp). A curva Receiver Operating Characteristic (ROC) e a Área Sob a Curva (AUCs) também foram plotadas e usadas para avaliação. Os resultados das métricas foram ACC = 0,9950, Sen = 99,16% e Sp = 99,89%.

Palavras-chave: Imagens de TC; Redes Neurais Convolucionais; COVID-19; Wavelets; WCNN-COVID.

Resumen

A fines de 2019, surgió un nuevo tipo de coronavirus en China y se denominó SARS-CoV-2. Primero impactó en el país donde surgió y luego se extendió por todo el mundo. El SARS-CoV-2 es la causa de la enfermedad COVID-19 que deja impresiones características en las imágenes de TC de tórax de pacientes infectados. En este artículo, proponemos un modelo de clasificación, basado en CNN y transformada wavelet, para clasificar imágenes de pacientes con COVID-19. Se llamó WCNN-COVID. El modelo fue aplicado y probado en repositorios de imágenes TC abiertos y privados. Se procesaron 25534 imágenes de 200 pacientes. La matriz de confusión se generó calculando la Precisión (ACC), la Sensibilidad (Sen) y la Especificidad (Sp). La curva característica operativa del receptor (ROC) y el área bajo la curva (AUC) también se trazaron y utilizaron para la evaluación. Los resultados métricos fueron ACC = 0,9950, Sen = 99,16 % y Sp = 99,89 %.

Palabras clave: Imágenes de TC; Redes Neuronales Convolucionales; COVID-19; Wavelets; WCN-COVID.

1. Introduction

The first official COVID-19 (COronaVIrus Disease 2019) case was of a patient hospitalized in Wuhan, province of Hubei, China, on December 12, 2019. Nonetheless, retrospective studies identified a clinical case with the same symptoms of the disease back on December 1st, 2019. Exams showed the existence of a virus in the patient's lung fluids, which led to the discovery of a new coronavirus (CoV) which belongs to the Coronaviridae family. It was initially called Wuhan coronavirus (WHCV), then, 2019-nCoV, then, finally, SARS-CoV-2.

Coronaviriadae can cause respiratory, enteric, liver, and neurological diseases in domestic animals and persons (Zhu et al., 2011). They also have a phylogenetic relation to coronaviruses that cause severe acute respiratory syndrome (SARS) and Middle East Respiratory Syndrome (MERS) (Zhu et al., 2020). COVID-19, SARS, and MERS had a zoonotic origin, and bats, civets, and camels, respectively transmitted their virus.

Due to the COVID-19 global pandemic impact, there have been made international efforts toward simplifying the access to viral data and metadata through data repositories around the world, such 2019 Novel Coronavirus Resource (2019nCoVR) (Wu., 2013) and the National Center for Biotechnology Information (NCBI) (Sherry, et al., 2001). The more accessible the information is, the more likely it is that a set of medical countermeasures be developed quickly to control the disease around the world, as has happened with other diseases on other occasions (dos S Ribeiro, et al., 2018; Simon et al., 2005; Ribeiro et al., 2018). Research in medical image processing is being performed to classify radiology image and clinically aid with the disease prognostic for patients who develop lung infection, using chest X-ray images or computed tomography (CT) scans (Zhang et al., 2020; Ozturk et al., 2020; Dai, et al., 2020). Radiology images show similarities amongst COVID-19 patients and some other type of viral pneumonia, namely SARS and MERS. In the medical image processing field, research were conducted to develop machine learning methods to classify image COVID-19, either using CT scan images or chest X-ray ones (Zhang et al., 2020; Ozturk et al., 2020; Sethy & Behera, 2020; Wang & Wong, 2020; Abbas et al., 2020; Narin et al., 2020; Bassi & Attux, 2020; Chen, et al., 2020; Wu, et al., 2020; Yang, et al., 2020).

Deep learning is a machine learning technique and has been used in research with radiology images since early Artificial Intelligence development stages (Zhang et al., 2020; Sethy & Behera, 2020; Wang & Wong, 2020; Abbas et al.,

2020; Chen, et al., 2020). It allows computer models to learn how to represent data in various levels of abstraction and layers of processing (Zhang et al., 2020; LeCun et al., 2015; Martin, et al., 2020). Radiology images of patients with COVID-19 presents common features that might show a pattern, but this pattern it is not visible for radiologist, so deep learning can be an effective tool to aid specialists to analyze great volumes of data generated by CT images (Zhang et al., 2020; Martin, et al., 2020).

To create a model that achieves high measures of accuracy, we optimize the classification process in such way the wavelet transform decomposes and extracts images features. To determine the accuracy of the model, we classify CT images of patients affected by COVID-19. The images were obtained both from open and private repositories whose are further described. As the wavelet transform step is quite relevant, our model is named Wavelets and Convolutional Neural Network (WCNN-COVID).
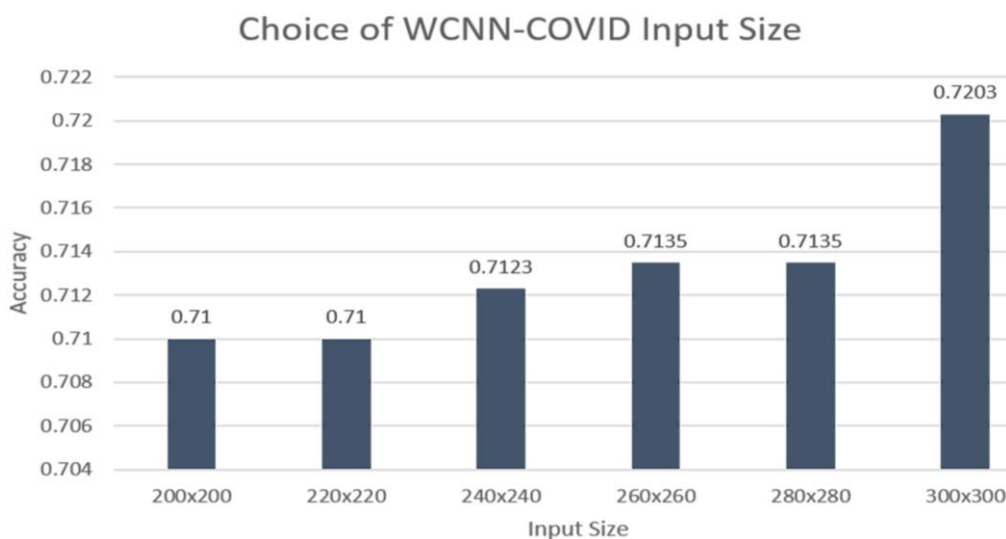
2. Methodology

The methodology for development of WCNN-COVID was created based on ideas inspired in the work of (Guo, Seyed Mousavi, Huu Vu, & Monga, 2017) and consists of five steps bellow.

First step: preparing the development environment. WCNN-COVID was programmed and trained in Python language with Keras library (Chollet, 2016). The model was developed using a I7-8750H Intel processor, 2.21GHz CPU, 16.0 GB RAM and a GeForce GTX 1060 graphic card with Max-Q Design.

Second step: Defining the network parameters. In the first training, weights are initialized randomly. The network was trained as per the ADAM model (Wani, Bhat, Afzal, & Khan, 2020). Standard parameters $\beta_1 = 0.9$ and $\beta_2 = 0.999$ were used (Kingma & Ba, 2014), as well as the initial learning rate $\alpha = 0.001$ reduced by a factor of 10. To choose the input parameters suitable values and the batch size of WCNN-COVID, several tests were performed using the images repository of the Hospital São Lucas, from PUCRS. The tests considered the computation capacity of the available hardware. For 200x200 and 220x220 entries, the lot size was 20. For larger entries, the batch-size was 10. The input tests were performed in 100 epochs. The test that obtained the best accuracy result was the one that considered a 300x300 input and batch-size of 10, as depicted in Figure 1.
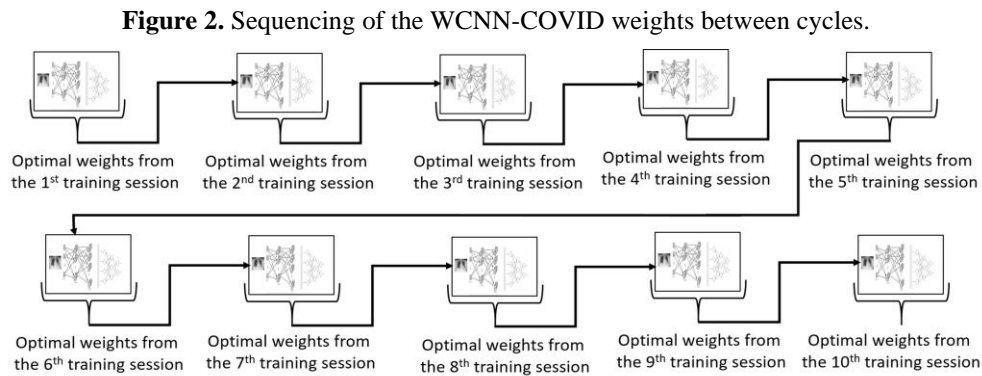
Figure 1. Choice of WCNN-COVID Input Size (200x200, ..., 300x300).

Source: Created by authors.

Third step: image pre-processing is responsible to generate the WCNN-COVID input. The images are decomposed into 3 approximate coefficients, horizontal and diagonal using the discrete wavelet transform Coiflet 5 family, with one level of decomposition. The combination of the coefficients creates a new digital image in which the Red, Green, and Blue (RGB) channels are replaced by the approximate, horizontal, and diagonal coefficients, respectively.

Fourth step: network training. The network was trained through 10 training and testing cycles. In each cycle, the training and test bases were created, randomly selecting COVID and NON-COVID images from the available bases. The proportion of 70% of the images was respected for training, 15% for testing and 15% for validation. In the validation stage, the weights obtained by carrying out the tenth training and test cycle were considered. According to the progression of the cycles, the weights of the lowest error rate, or the highest accuracy value in training are used to start it up in the subsequent cycle. For example, the weights of the first cycle were used to initialize the network in the second cycle, and so on. This technique contributed to increase the accuracy of the model. Figure 2 illustrates our weight transfer strategy between cycles.

Figure 2. Sequencing of the WCNN-COVID weights between cycles.

Source: Created by the authors.

Fifth step: Calculating the metrics used to measure the performance of the WCNN-COVID model. These metrics are commonly used to assess the performance of classification algorithms (Ruuska, et al., 2018; Skansi, 2018; Khatami et al., 2017). There is a standard way to show the number of true positives (TP), false positives (FP), true negatives (TN) and false negatives (FN) to be more visual. This method is called confusion matrix. For a classification of two classes, the confusion matrix is presented on Table 1.

Table 1. Example of a confusion matrix.

	Classifier says YES	Classifier says NO
In reality YES	True positives	False positives
In reality NO	False negatives	True negatives

Source: Adapted from Skansi (2018).

The confusion matrix allows to determine the following metrics (Narin et al., 2020; Ruuska, et al., 2018; Skansi, 2018; Khatami et al., 2017):

- Accuracy (ACC): accurate classification rate as per the total number of elements calculated by

$$ACC = \frac{TN + TP}{TN + TP + FN + FP}$$

- Sensitivity (Sen): true positive rate calculated by $Sen = \frac{TP}{TP+FN}$

- Specificity (Sp): true negative rate calculated by $Sp = \frac{TN}{TN + FP}$
- Receiver Operating Characteristic Curve (ROC curve): ROC accuracy ratio is a common technique for default probability models accuracy judging (Shirazi et al., 2018).

3. Related Work

WCNN-COVID was conceived to handle CT images; nonetheless, in this section we considered related works on dealing COVID-19 using chest CT images. Research papers (Chen, et al., 2020; Wu, et al., 2020; Yang, et al., 2020; Ozkaya et al., 2020; Barstugan et al., 2020; Wang, et al., 2020; Chen(a), et al., 2021) proposes to classify pneumonia caused by COVID-19 in computed tomography (CT) images. All these papers were based on deep learning models, either a new model was developed, or a transfer learning technique was used in pre-existing models. The chest CT image repositories used were from different locations:
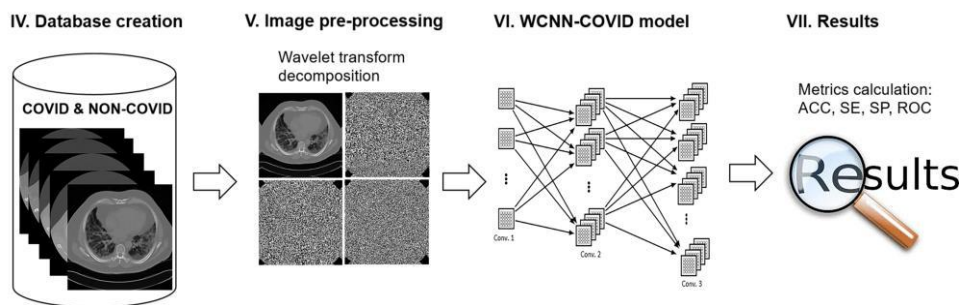
- Renmin Hospital of Wuhan University (RHWU) (Chen, et al., 2020; Wu, et al., 2020).
- The First Hospital of China Medical University (1st HCMU) (Wu, et al., 2020).
- The Fifth Affiliated Hospital of Sun Yat-sen University (Chen(a), et al., 2021).
- Beijing Youan Hospital (BYH) in China (Wu, et al., 2020).
- Shanghai Public Health Clinical Center (Yang, et al., 2020).
- Societa Italiana di Radiologia Medica e Interventistica (Ozkaya et al., 2020; Barstugan et al., 2020).
- Picture Archiving and Communication System (PACS) from the radiology department (Union Hospital, Tongji Medical College, Huazhong University of Science and Technology) (Wang, et al., 2020).

These papers presented various results, for instance, as far as accuracy was concerned, the lowest accuracy value was 76%, and the highest, 99.68%.

4. The WCNN-COVID model

The WCNN-COVID was created to integrate the digital image pre-processing and processing by decomposing images using wavelet transform and machine learning with deep neural networks. Such integration happened aiming at better accuracy and classification optimization. The following subsections describe both the integration workflow and the components and techniques used. We can see the integration workflow presented on Figure 3.

Figure 3. Diagram of the proposed methodology to classify COVID-19.

Source: Created by authors.

The next section presents the activities of WCNN-COVID's database creation.

5. Database Creation

The database used to train and evaluate the WCNN-COVID is composed by 200 patients, subdivided into two sub-databases: i) COVID, composed by 100 positively tested patients for COVID-19; and ii) NON-COVID, composed by 100 negatively tested patients. The images patient came from five repositories, being four open source and one private:

• COVID-19 CT scans data set (KAGGLE) (Maranhão, 2020).

• MosMedData dataset: COVID19_1000 Dataset (MosMedData, 2020).

• NIH Clinical Center dataset: dataset of 32,000 CT images (Summers, 2020).

• Data set UESTC-COVID-19 (Wang(d), et al., 2020).

• COVID-19 (private) data set formed by CT images from PUCRS Hospital São Lucas (HSL-PUCRS). As this repository is from a private university, we submitted a request to its respective Ethics Committee Board (ECB) to use the images. ECB analyses our demand, approved it, granted us access and give us the Certificate of Presentation of Ethical Appreciation number 30791720.5.0000.5336.

From the set of 100 patients of the COVID sub-base, 70% of them were used in training phase, 15% in test phase and the remaining 15% used in validation phase. The same distribution was made in the sub-base NON-COVID, as shown in Table 2. The patient images used in training were not used again in testing and validation, that is, the patients were disjointedly divided.

Table 2. Distribution of images in databases used by WCNN-COVID.

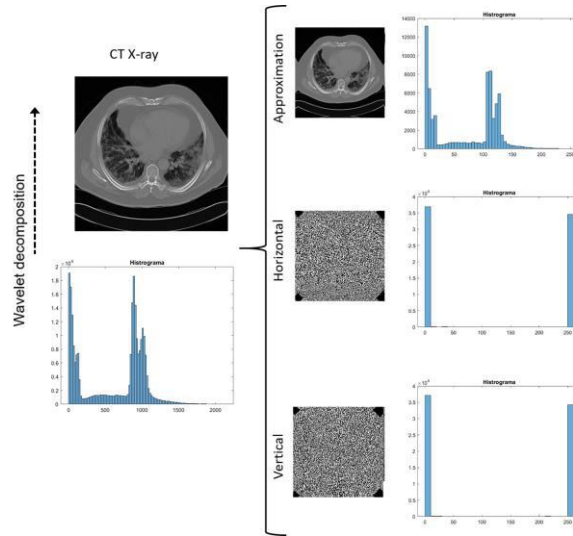| Sub-base	Patients/ images	Training patients/images	Test patients/images	Validation patients/images
COVID	100/12767	70/8937	15/1915	15/1915
NON-COVID	100/12767	70/8937	15/1915	15/1915

Source: Created by authors.

Once the creation of the database is completed, images pre-processing tasks are performed as detailed in the next section.

6. Wavelet

The wavelet transform was used for image multiscale decomposition so that different scales can be manipulated and inserted as an input for WCNN-COVID. Moreover, training in wavelet domain can boost up the training and testing procedures. Using wavelet coefficients encourages activation sparsity in hidden layers, as well as in the output layer. Moreover, by using residuals, wavelet coefficients themselves become sparser and, therefore, easier for the network to learn sparse maps rather than dense ones. The histograms in Figure 4 illustrate the sparse distribution of the horizontal, vertical, and approximation coefficients. This high level of sparsity further reduces the training time required for the network and it results in more accurate classification results (Guo et al., 2017).

Figure 4. Example of histogram from the original image and corresponding horizontal, vertical, and approximation coefficients.

Source: Created by authors.

The wavelet theory is referred as a wavelet at different scales and positions. The Discrete Wavelet Transform (DWT) can be regarded as a sequence of numbers which sample a certain continuous function. When digital images are handled at multiple resolutions, the DWT is a viable mathematical tool. In addition to its efficient and highly intuitive framework to represent and store multiresolution images, the DWT provides powerful insights into an image's spatial and frequency characteristics (Rafael, 2006; Jansen, 2012; Williams & Li, 2016). Given the following image, $f(a, b)$, the DWT bidimensional transformation pair is defined as (Rafael, 2006; Jansen, 2012; Williams & Li, 2016):

$$Wf(a,b) = \int_{-\infty}^{+\infty} f(t)\psi_{a,b}(t)dt \quad (1)$$

For a discrete signal of N points, the integral above can have an approximate value from a summation, such as:

$$Wf(a,b) = \sum_{t=0}^{N-1} f(t)\psi_{a,b}(t) \quad (2)$$

Function $\psi_{a,b}(t)$, called wavelet, is a derivative from a function $\psi(t)$ through the following transformation:
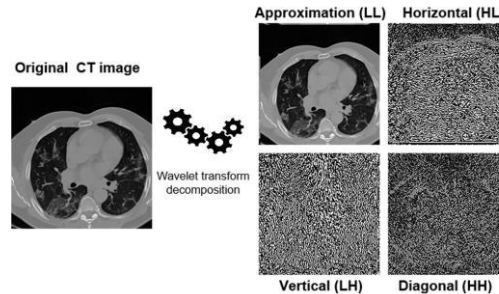
$$\psi_{a,b}(t) = \frac{1}{\sqrt{a}}\psi\left(\frac{t-b}{a}\right) \quad (3)$$

where $a \in R^+$, $b \in R$ and $\psi\left(\frac{t-b}{a}\right)$ are the base of the wavelet. Where b represents the wavelet position or translation and a is called the scale parameter associated to the width of the window. There is a wide range of choice for function $\psi(t)$, called mother wavelet e.g. Daubechies, Symlets, Coiflet, amongst others. The scaled and shifted versions of this mother wavelet correspond to bandpass filters with different bandwidths and different time durations. The wavelet transform runs a transform stage in every row, thus yielding a matrix; the left side contains down sampled lowpass (L) coefficients of every row and the right side contains the high-pass (H) coefficients. Then, it is applied to every column resulting in four types of coefficients, as per Figure 5 (Rafael, 2006; Jansen, 2012; Williams & Li, 2016).

•   Coefficients that result from a convolution with high pass in both directions (HH) represent diagonal features of the image.

•   Coefficients that result from a convolution with high pass on the columns after a convolution with low pass on the rows (HL) correspond to horizontal features of image structures.

•   Coefficients from high pass filtering on the rows, followed by low pass filtering of the columns (LH) reflect vertical features information.

• Coefficients from low pass filtering in both directions further processed in the next step reflect approximation information.

Figure 5. Overall diagram of *Wavelet* transform.

Source: Created by authors.

A. Analysis of Decomposition Coefficients

The analysis used a sample of 500 images from the COVID database and 500 images from the NON-COVID database. The Friedman test was used to assess significance for these two classes, as this is a heterogeneous, independent, and non-parametric dataset (Zimmerman & Zumbo, 1993; Ishitaki, Oda, & Barolli, 2016). This statistic test was applied to verify whether the classes present values which are statistically similar when compared to one another, and about each coefficient resulting from wavelet decomposition (approximation, horizontal, vertical, and diagonal coefficients from the corresponding images). Version 5.3 of BioEstat, a biostatistical analysis software, was used to input hypothesis and significance tests and data.
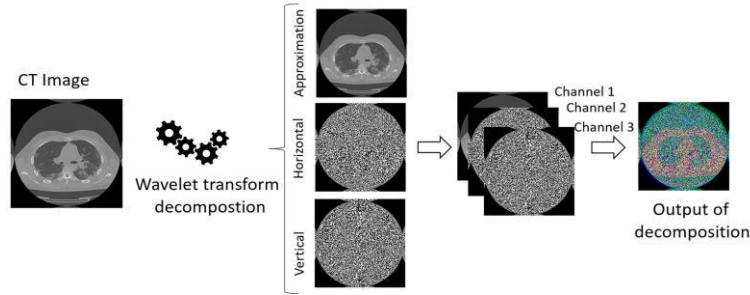
All tests considered $\alpha = 0.05$. For the Friedman analysis, the standard deviation from the wavelet decomposition (standard deviation of the approximation, horizontal, vertical, and diagonal coefficients) highlighted that every wavelet coefficient standard deviation from the COVID database images compared with the NON-COVID database images has presented significant statistical differences, except for the diagonal coefficient. Thus, the three coefficients (approximation, horizontal, and vertical) were used as inputs for WCNN-COVID, for they presented more statistically significant intergroup differences.

B. Mother Wavelet and Decomposition Level

The decision to associate Coifltes 5 with WCNN was taken based on the work of   work of (da Costa Junior & Patrocinio, 2019) in which wavelets were used to reduce noise in dense breast radiography images. In the mentioned work, the wavelet transforms of the Daubechies, Symlets, Coiflets, Fejer-Korovkin and dMeyer families were tested, and the Coiflets 5 family presented the best noise reduction results. Thus, in an analogous way, we associate the Coiflets 5 family to the WCNN model. In addition, we chose to define a decomposition level to avoid loss of information needed for image classification

Thus WCNN-COVID model development used the Coiflets family. Coiflets are also build by I. Daubechies on the request of R. Coifman wavelets are orthogonal compactly supported wavelets with the highest number of vanishing moments for both the wavelet and scaling function for a given support width. The Coiflet wavelets are more symmetric and have more vanishing moments than the Daubechies wavelets (Merry, 2005). The Coiflets family approximation, horizontal, vertical, and diagonal coefficients can be used to infer more structural information about the image. Hence, three coefficients were selected for WCNN-COVID input - approximation, horizontal, and vertical - and generated by Coiflet 5 mother wavelet in one level of decomposition, as per Figure 6.

Figure 6. *Wavelet* decomposition process.

Source: Created by authors.

According to He and Sun (He & Sun, 2015), convolutional layers represent usually 90-95% of the computational cost. The computational complexity of convolutional layers was analyzed here. For a given CNN, the total complexity of all convolutional layers can be represented as:

$$O\left(\sum_{l=1}^{d} n_{l-1} \cdot s_l^2 \cdot n_l \cdot m_l^2\right) \qquad (4)$$

Here, l is the index of a convolutional layer, and d is the depth (number of convolutional layers); n_l is the number of filters (also known as "width") in the l-th layer; n_{l-1} is also known as the number of input channels of the l-th layer; s_l is the spatial size (length) of the filter; m_l is the spatial size of the output feature map. For this paper, the WCNN-COVID input is the image resulting from the wavelet transform. That means, the input image is half the spatial resolution of the original image. Thus, m_l (the spatial size of the output feature map) is also reduced in half. So, the WCNN-COVID complexity is reduced by 50% compared with a conventional CNN using original images and without the wavelet transform decomposition.

7. WCNN-COVID Model

A CNN is composed of two stages: feature extraction stage and classification stage. In the CNN, the pooling and convolution layers act as a stage of feature extraction, whereas the classification stage is made of one or more fully connected layers followed by a sigmoid function layer (Wani et al., 2020), which are presented below.

A new convolution operation was created for the convolutional layer, in which a kernel is used to map the activations from one layer into the next. The convolution operation places the kernel in each possible position in the image (or hidden layer) so that the kernel overlaps the entire image and executes a dot product between the kernel parameters and its corresponding receptive field - to which a kernel is applied - in the image. The convolution operation is executed in every region the image in order to define the next layer (in which activations keep their spatial relations in the previous layer) (LeCun et al., 2015; Aggarwal & others, 2018; Ponti & da Costa, 2018). There may be several kernels in the convolutional layer. Every kernel uncovers a feature, such as an edge or a corner. During the forward pass, every kernel is slid to the width and the height of the image (or hidden layer), thus generating the feature map (LeCun et al., 2015; Balas et al., 2019; Aggarwal & others, 2018; Ponti & da Costa, 2018).

WCNN-COVID uses Adaptive Moment Estimation (ADAM), an adaptive optimization technique which saves an exponentially decaying average of previous squared gradients v_t. In addition to that, ADAM also computes the average of the second moments of the gradients m_t (Wani, Bhat, Afzal, & Khan, 2020; Kingma & Ba, 2014). Average and non-centered variance values m_t are presented in (5) and (6), respectively:

$$m_t = \beta_1 m_{t-1} + (1 - \beta_1)gt \quad (5)$$
$$v_t = \beta_2 v_{t-1} + (1 - \beta_2)gt^2 \qquad (6)$$

ADAM updates exponential moving averages of the gradient and the squared gradient where the hyperparameters β1, β2 ∈ [0, 1] control the decay rates of these moving averages (7) and (8):

$$\widehat{m}_t = \frac{m_t}{1-\beta_1^t} \qquad (7)$$

$$\hat{v}_t = \frac{v_t}{1-\beta_2^t} \qquad (8)$$

The final equation for update is presented in (9):

$$w_{t+1} = w_t - \frac{\alpha.\widehat{m}_t}{\sqrt{\hat{v}_t}+\epsilon} \qquad (9)$$

where α is the learning rate and ϵ is a constant added to the denominator for quick conversion methods in order to avoid the division by 0 (Wani et al., 2020; Kingma & Ba, 2014).

WCNN-COVID uses the Dropout technique, the most popular technique to reduce overfitting. Dropout refers to dropping out neurons in a neural network during training. Dropping out a neuron means temporarily disconnecting it, as well as all its internal and external connections, from the network. Dropped-out neurons neither contribute to the forward pass nor do they contribute to the backward pass. By using the dropout technique, the network is forced to learn the most robust features as the network architecture changes with every input (Balas et al., 2019; Wani et al., 2020).

The output of every convolutional layer is fed by an activation function. The activation function layer consists of an activation function which uses the feature map produced by the convolutional layer and generates the activation map as the output. The activation function is used to change a neuron activation level in an output signal. Thus, it performs a mathematical operation and generates the neuron activation level at a specific interval, for instance, 0 to 1 or -1 to 1 (Wani, Bhat, Afzal, & Khan, 2020). The functions used were the following:
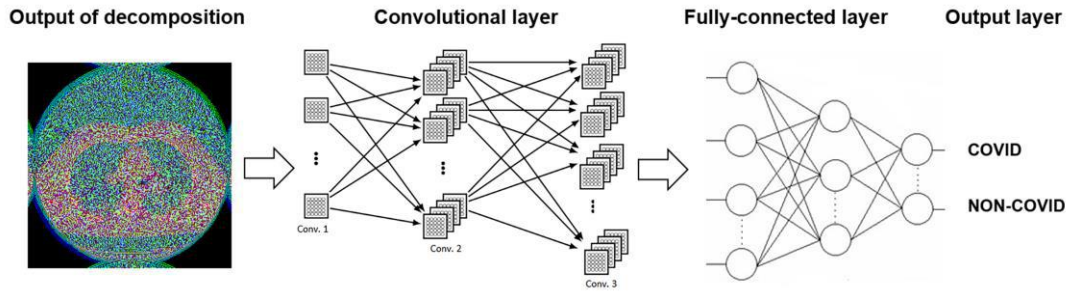
•   Sigmoid / Logistic activation function: The sigmoid function $\sigma(x) = \frac{1}{1+e^{-x}}$ is a curve shaped like an S (Ponti & da Costa, 2018).

•   The activation function $f(x) = max(0, x)$ is called Rectified Linear Unit – ReLU (Ponti & da Costa, 2018) and generates a non-linear activation map.

The pooling layer, or down sampling layer, is used to reduce the receptive field spatial size, thus reducing the number of network parameters. The pooling layer selects a reduced sample of each convolutional layer feature map. Max-pooling was the technique used for this work; it generates the maximum value in the receptive field. The receptive field is 2x2, therefore, max-pooling will issue the maximum of the four input values (Wani et al., 2020).

After the convolution and pooling processes, the next step is to add one or more fully connected layers at the end. In the fully connected layer, each neuron from the previous layer is connected to each neuron from the following layer, and all the values contribute to predict how strong a value correlates to a given class (Wani et al., 2020). The fully connected layers may be layered on top of one another to learn even more sophisticated combinations of features. The output of the last fully connected layer is fed by an activation function which generates the class scores. The sigmoid activation function is the one used for WCNN-COVID. It produces class scores, and the class with the highest score is treated as the correct one (Wani et al., 2020).

Convolutional Neural Networks (CNNs) were proposed to assess image data. The name comes from the convolution operator, an easy way of doing complex operations using the convolution kernel (Ravì, et al., 2016). Many variations of the CNN were proposed, such as AlexNet (Krizhevsky et al., 2012), Clarifai (Zeiler & Fergus, 2014), GoogleNet (Szegedy, et al., 2015). The WCNN-COVID structure is also a variation of a CNN which contains a pre-processing stage with a *wavelet* transform and the following architecture: an input layer, a convolutional layer, a dense layer, and an output layer, as per Figure 7.

Figure 7. WCNN-COVID classification scheme.

Source: Created by authors.

The WCNN-COVID detailed architecture to classify an image as COVID-19 is illustrated in Table 3. The network consists of conventional layers, including the input layer, the convolution layer, the max-pooling layer and the fully-connected layers. Besides, a rectified linear unit (ReLU) activation function is used after each convolution layer (1st, 3rd, 5th and 7th) and dense layers (9th, 10th, 11th and 12th). In order to reduce the possibility of overfitting, a dropout rate of 20% was implemented to the first four fully-connected layers (9th, 10th, 11th and 12th).

Table 3. WCNN-COVID architecture. The network contains the input (I), the convolution (C), the max-pooling (M) layers and the fully connected network (F).

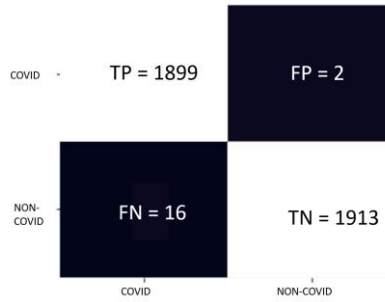| Layer		WCNN-COVID	
Filter	Dimensions	Input/Output	Dimensions
0	I		300x300x3
1	C	5x5x256	296x296x256
2	M	2x2	148x148x256
3	C	3x3x128	146x146x128
4	M	2x2	73x73x128
5	C	3x3x64	71x71x64
6	M	2x2	35x35x64
7	C	3x3x32	33x33x32
8	M	2x2	16x16x32
9	F	16x16x32x256	1x256
10	F	1x1x256x128	1x128
11	F	1x1x128x64	1x64
12	F	1x1x64x32	1x32
13	F	1x1x32x1	1x1

Source: Created by authors.

8. Results

In this section we present the results of the application of WCNN-COVID according to parameters, data, methodology and metrics described in above sections.

Through the WCNN-COVID weight evolution as described in the previous section, the WCNN-COVID from the last training session was chosen to be applied in the validation phase. Thus, the confusion matrix was generated with 1915 images from the COVID sub-base and 1915 images from the NON-COVID sub-base. This resulted in a total of 3830 images for validating WCNN-COVID. Therefore, as per the confusion matrix from Figure 8, we can see that i) true positives (TP) = 1899;

ii) true negatives (TN) = 1913; iii) false positives (FP) = 2; and iv) false negatives (FN) = 16.

Figure 8. WCNN-COVID confusion matrix.

Source: Created by authors.

Using the TP, TN, FP and FN parameters, the following metrics were calculated: accuracy, sensitivity, specificity, and F1 Score, as per Table 4.

Table 4. metrics RESULTS.

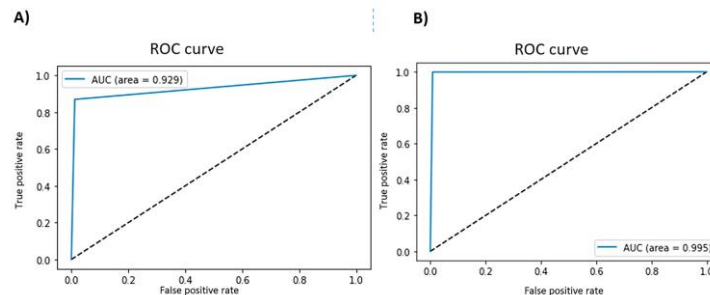| Class	Accuracy	Recall /sensitivity	Specificity
COVID-19	0,9953	0,9916	0,9989

Source: Created by authors.

To evaluate the methodology performance used in input images pre-processing tasks, through the wavelet transform – which decomposes the image into 4 sub-images –, different networks were trained using the COVID and NON-COVID image repositories, with and without pre-processing.

The ROC curves for the two tests were constructed. The first test did not use the described methodology intended to pre-process and to decompose images using wavelet, as illustrated in Figure 9(A). However, the second test followed all the image pre-processing, as shown in Figure 9(B).

The ROC curve A and ROC curve B were calculated in the validation stage of the tenth training and test cycle. Thus, based on the analysis of the ROC curves, the area of the curve without preprocessing is 0.9229 and the area of the curve with preprocessing is 0.9950, as shown in Figure 9.

Figure 9. WCNN-COVID ROC curves: A) Data Set without *wavelet*/AUC = 0.9229 B) Data Set with *wavelet*/AUC=0.995.
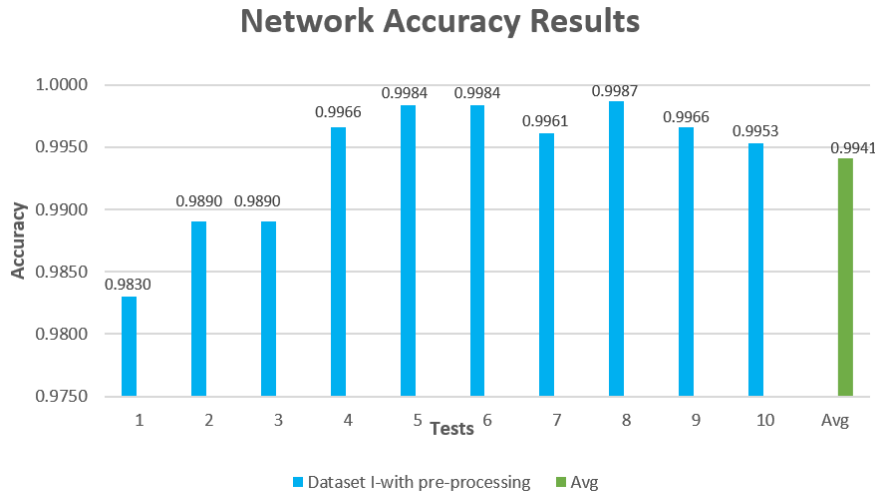

Source: Created by authors.

For every 10 training and testing cycles, 1000 epochs were applied. This generated the following result: the lowest accuracy was 0.9830 and the highest, 0.9987. A média geral do teste para WCNN-COVID mostrou acurácia de 0,9953 e

desvio padrão de 0.005284, conforme Figura 10.

Figure 10. WCNN-COVID results: results for each test and overall average (avg) of all 10 tests.
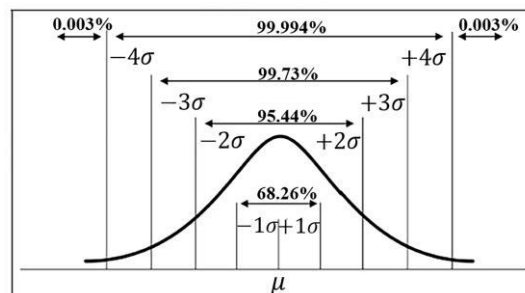

Source: Created by authors.

It was also confirmed that the image classification as COVID or NON-COVID follow the normal distribution. The continuous variable (x) represents success or failure when classifying images and the probability density function is denoted by Equation (9), as follow (Pinheiro et al., 2009):

$$f(x) = \frac{1}{\sqrt{2\pi\sigma^2}} \cdot e^{-\frac{1}{2}\left(\frac{x-\mu}{\sigma}\right)^2} \qquad (9)$$

Normal distribution is described by the following parameters: average (μ) and standard deviation (σ); the value of $(x) \in (-\infty, \infty)$, as well as the curve is represented in Figure 11 which also includes important areas, the total area under the curve being 1 (Pinheiro et al., 2009).

Figure 11. Normal distribution typical curve.

Fonte: Pinheiro et al., (2009)

To calculate the area under the normal curve, a standardized normal distribution, also known as folded normal distribution, is used. It is the normal distribution with $\mu = 0$ and $\sigma = 1$. Given that $\sigma \cong 0.005284$ for accuracy, when the value of the normal distribution area of the curve standardized between 0 and σ, considering $\mu = 0$, is calculated, the result is the probability of an image being wrongly classified by the model. This can be calculated by the normal probability function

$P(x)$, as per Equation (10).

$$P(x) = \int_a^b \frac{1}{\sqrt{2\pi\sigma^2}} . e^{-\frac{1}{2}\left(\frac{x-\mu}{\sigma}\right)^2} dx \quad (10)$$

So we found $(x) \cong \int_0^{0,005284} \frac{1}{\sqrt{2\pi}} . e^{-\frac{1}{2}x^2} dx \cong \mathbf{0,00210}$. That said, there is a 0.210% chance the image be classified incorrectly, which denotes the high trustworthy of our model.

The validation result step in the tenth cycle of training and testing was compared with the state-of-the-art methods presented in Section 3. The best ACC result was 99.53%, as shown in bold in Table 5.

Table 5 - Comparison of WCNN-COVID with state-of-the-art methods (chest computed tomography - CT).

Methods	Type	ACC	Sen	Sp
(Wu, et al., 2020) Xiangjun Wu et al.	CT	0.7600	0.8110	0.6150
(Wang, et al., 2020) Xinggang Wang et l.	CT	0.9010	0.8400	0.9820
(Yang, et al., 2020) Shuyi Yang et al.	CT	0.9200	0.9700	0.8700
(Chen(a), et al., 2021) Hongtao Chen(a) et al.	CT	0.9408	0.9487	0.8846
(Chen, et al., 2020) Jun Chen et al.	CT	0.9524	1.000	0.9355
(Ozkaya, Ozturk, & Barstugan, 2020) Umut Ozkaya et al.	CT	0.9827	0.9893	0.9760
(Barstugan, Ozkaya, & Ozturk, 2020) Mucahid Barstugan et al.	CT	**0.9968**	0.9772	0.9967
WCNN-COVID model	X-ray	**0.9953**	0.9916	0.9989

Source: Created by authors.

9. Discussion

The results shows that WCNN-COVID model has relevant performance for medical digital images processing and some applications area, including:

1.   Predictability and trust.

2.   Unprecedented accuracy amongst classification models which use convolutional neural networks.

3.   Outcomes with few tests. The trust in the results of a method or a technique is an indispensable characteristic in a classification model. It is crucial that images classification be trustworthy.

It is important to carefully choose the approaches and parameters that the network will use during its execution. About the adaptive learning rate optimizer, our option fell on the ADAM algorithm. This algorithm leverages both AdaGrad and RMSProp, whose are the ability of dealing with sparse gradients and non-stationary objectives respectively (Wani et al., 2020). Beyond that the method is straightforward to implement and requires low memory levels to execute.

The standard image size generated by CT scans equipment's is 512x512 pixels. Therefore, it was necessary to conduct a study to identify the size to which the original CT images should be converted to fit the WCNN-COVID input parameters. We observed that the higher the input size, the more accurate the network was, therefore more studies should be conducted to validate or to refute that empirical observation. As showed in Figure 1, when the input size was 300x300, the accuracy was 0.7203.

The model that uses image pre-processing provides rapid convergence of the network weights. The convergence indicates that the wavelet decomposition, in the pre-processing phase, contributes to obtaining the best weights during the training and testing phases of the model. The execution of the 10 training and test cycles also contribute to assess the stability of the model's accuracy values.

The average ACC value from the 10 training and test cycles was 0.9941. Besides, it is worth mentioning that the

accuracy of all tests went over 0.98. The weights used by WCNN-COVID in the 10th training session were used in the validation step, and the ACC value was 0,9953. The WCNN-COVID input was sub-images generated from the *wavelet* decomposition coefficients which are half the resolution size of the original image. Thus, the spatial size of the output feature map is also reduced in half which accelerates the classification process. Moreover, using *wavelet* coefficients encourages activation sparsity in hidden layers as well as in output layer. Moreover, by using residuals, *wavelet* coefficients themselves become sparser and therefore easier for the network to learn sparse maps rather than dense ones, thus speeding up the WCNN-COVID classification process.

The *wavelet* decomposition in the pre-processing input network contribute to WCNN-COVID training performance and high accuracy of model proposed in Figure 9A and Figure 9B. Figure 9A depicts that the area of the ROC curve for tests with images without preprocessing is 0.9229 and Figure 9B shows that the area of the ROC curve using preprocessing is 0.9950, which represents an increase of 7.8% in the tests, using pre-processing in relation to the ROC curve area of the tests using images without pre-processing.

10. Conclusion

This paper proposed and validated a new automated classification model called WCNN-COVID. It is based on a deep neural network using *wavelet* transform to extract features to classify image patients with COVID-19, who already present lung changes (or pneumonia). The WCNN-COVID results have shown that analyzing CT images using deep learning methods have provided quick and highly accurate results, when applied to classify pneumonia caused by COVID-19. The automated classification results were calculated separately for the testing and validation steps. The proposed model was used to classify a set of real images selected from repositories both public and private. A total of 10 training and test cycles were performed.

The results we obtained with this work indicates that the association of CNNs and transform *wavelet*s is promising for creating classification models. That way, beyond the scope of this work, we are principally committed with further research involving neural network improvements, using the model to rather classify medical digital images of others specialties than pulmonary diseases, and furthermore, using the model in specific images of several areas such as agriculture and metallurgy.

11. Conflict of Interest and Ethical Standards

All authors declare no conflict of interest, and this article does not contain studies with human or animal participants performed by any of the authors.

Acknowledgements

References

Abbas, A., Abdelsamea, M., & Gaber, M. (2020, 4). Classification of COVID-19 in chest X-ray images using DeTraC deep convolutional neural network. https://doi.org/10.1101/2020.03.30.20047456

Aggarwal, C. C., & others. (2018). *Neural networks and deep learning*. Springer https://doi.org/10.1007/978-3-319-94463-0

Balas, V. E., Roy, S. S., Sharma, D., & Samui, P. (2019). *Handbook of deep learning applications* (Vol. 136). Springer. https://doi.org/10.1007/978-3-030-11479-4

Barstugan, M., Ozkaya, U., & Ozturk, S. (2020). Coronavirus (covid-19) classification using ct images by machine learning methods. *arXiv preprint arXiv:2003.09424*.

Bassi, P. R., & Attux, R. (2020). A Deep Convolutional Neural Network for COVID-19 Detection Using Chest X-Rays. *arXiv preprint arXiv:2005.01578*.

Chen(a), H., Guo, S., Hao, Y., Fang, Y., Fang, Z., Wu, W., & Li, S. (2021). Auxiliary Diagnosis for COVID-19 with Deep Transfer Learning. *Journal of Digital Imaging*, 1–11.

Chen, J., Wu, L., Zhang, J., Zhang, L., Gong, D., Zhao, Y., et al. (2020). Deep learning-based model for detecting 2019 novel coronavirus pneumonia on high-resolution computed tomography: a prospective study. *MedRxiv*.

Chollet, F. (2016). Building powerful image classification models using very little data. *Keras Blog*. Retrieved from https://blog.keras.io/building-powerful-image-classification-models-using-very-little-data.html

Cui, J., Li, F., & Shi, Z.-L. (2019). Origin and evolution of pathogenic coronaviruses. *Nature Reviews Microbiology, 17*, 181–192. https://doi.org/10.1038/s41579-018-0118-9

da Costa Junior, C. A., & Patrocinio, A. C. (2019). Performance Evaluation of Denoising Techniques Applied to Mammograms of Dense Breasts. *XXVI Brazilian Congress on Biomedical Engineering*, (pp. 369–374).

Dai, W.-c., Zhang, H.-w., Yu, J., Xu, H.-j., Chen, H., Luo, S.-p., et al., (2020). CT imaging and differential diagnosis of COVID-19. *Canadian Association of Radiologists Journal, 71*, 195–200. https://doi.org/10.1177/0846537120913033

dos S Ribeiro, C., van Roode, M. Y., Haringhuizen, G. B., Koopmans, M. P., Claassen, E., & van de Burgwal, L. H. (2018). How ownership rights over microorganisms affect infectious disease control and innovation: A root-cause analysis of barriers to data sharing as experienced by key stakeholders. *PLoS One, 13*, e0195885. https://doi.org/10.1371/journal.pone.0195885

Guo, T., Seyed Mousavi, H., Huu Vu, T., & Monga, V. (2017). Deep wavelet prediction for image super-resolution. *Proceedings of the IEEE Conference on Computer Vision and Pattern Recognition Workshops*, (pp. 104–113).

He, K., & Sun, J. (2015). Convolutional neural networks at constrained time cost. *Proceedings of the IEEE conference on computer vision and pattern recognition*, (pp. 5353–5360).

Ishitaki, T., Oda, T., & Barolli, L. (2016). A neural network based user identification for Tor networks: Data analysis using Friedman test. *2016 30th International Conference on Advanced Information Networking and Applications Workshops (WAINA)*, (pp. 7–13). https://doi.org/10.1109/waina.2016.143

Jansen, M. (2012). *Noise reduction by wavelet thresholding* (Vol. 161). Springer Science & Business Media. https://doi.org/10.1007/978-1-4613-0145-5

Khatami, A., Khosravi, A., Nguyen, T., Lim, C. P., & Nahavandi, S. (2017). Medical image analysis using wavelet transform and deep belief networks. *Expert Systems with Applications, 86*, 190–198. https://doi.org/10.1016/j.eswa.2017.05.073

Kingma, D. P., & Ba, J. (2014). Adam: A method for stochastic optimization. *arXiv preprint arXiv:1412.6980*.

Krizhevsky, A., Sutskever, I., & Hinton, G. E. (2012). Imagenet classification with deep convolutional neural networks. *Advances in neural information processing systems*, (pp. 1097–1105).

LeCun, Y., Bengio, Y., & Hinton, G. (2015). Deep learning. *nature, 521*, 436–444. https://doi.org/10.1038/nature14539

Maranhão, A. (2020). *COVID-19 CT: scans20 CT scans and expert segmentations of patients with COVID-19*. Retrieved 02 02, 2021, from Kaggle: https://www.kaggle.com/andrewmvd/covid19-ct-scans

Martin, D. R., Hanson, J. A., Gullapalli, R. R., Schultz, F. A., Sethi, A., & Clark, D. P. (2020). A deep learning convolutional neural network can recognize common patterns of injury in gastric pathology. *Archives of pathology & laboratory medicine, 144*, 370–378. https://doi.org/10.5858/arpa.2019-0004-OA~

Merry, R. J. (2005). Wavelet theory and applications: a literature study. *DCT rapporten, 2005*.

MosMedData. (2020). *MosMedData: COVID19_1000 Dataset:Chest CT Scans with COVID-19*. Retrieved from https://mosmed.ai/en/

Narin, A., Kaya, C., & Pamuk, Z. (2020). Automatic detection of coronavirus disease (covid-19) using x-ray images and deep convolutional neural networks. *arXiv preprint arXiv:2003.10849*.

Ozkaya, U., Ozturk, S., & Barstugan, M. (2020). Coronavirus (COVID-19) Classification using Deep Features Fusion and Ranking Technique. *arXiv preprint arXiv:2004.03698*.

Ozturk, S., Ozkaya, U., & Barstugan, M. (2020). Classification of coronavirus images using shrunken features. *medRxiv*. https://doi.org/10.1101/2020.04.03.20048868

PINHEIRO, J. I., CUNHA, S. B., CARVAJAL, S. R., & GOMES, G. C. (2009). Estatística Básica: A arte de trabalhar com dados. Rio de Janeiro–RJ. *Estatística Básica: A arte de trabalhar com dados. Rio de Janeiro–RJ*. Editora Elsevier.

Ponti, M. A., & da Costa, G. B. (2018). Como funciona o deep learning. *arXiv preprint arXiv:1806.07908*.

Rafael, C. (2006). Gonzalez, and Richard E. Woods. *Digital image processing*.

Ravì, D., Wong, C., Deligianni, F., Berthelot, M., Andreu-Perez, J., Lo, B., & Yang, G.-Z. (2016). Deep learning for health informatics. *IEEE journal of biomedical and health informatics, 21*, 4–21. https://doi.org/10.1109/JBHI.2016.2636665

Ribeiro, C. d., Koopmans, M. P., & Haringhuizen, G. B. (2018). Threats to timely sharing of pathogen sequence data. *Science, 362*, 404–406. https://doi.org/10.1126/science.aau5229

Ruuska, S., Hämäläinen, W., Kajava, S., Mughal, M., Matilainen, P., & Mononen, J. (2018). Evaluation of the confusion matrix method in the validation of an automated system for measuring feeding behaviour of cattle. *Behavioural processes, 148*, 56–62. https://doi.org/10.1016/j.beproc.2018.01.004

Sethy, P. K., & Behera, S. K. (2020). Detection of coronavirus disease (covid-19) based on deep features. *Preprints, 2020030300*, 2020. https://doi.org//10.20944/preprints202003.0300.v1

Sherry, S. T., Ward, M.-H., Kholodov, M., Baker, J., Phan, L., Smigielski, E. M., & Sirotkin, K. (2001). dbSNP: the NCBI database of genetic variation. *Nucleic acids research, 29*, 308–311. https://doi.org/10.1093/nar/29.1.308

Shirazi, A. Z., Chabok, S. J., & Mohammadi, Z. (2018). A novel and reliable computational intelligence system for breast cancer detection. *Medical & biological engineering & computing, 56*, 721–732. https://doi.org/10.1007/s11517-017-1721-z

Simon, J. H., Claassen, E., Correa, C. E., & Osterhaus, A. D. (2005). Managing severe acute respiratory syndrome (SARS) intellectual property rights: the possible role of patent pooling. *Bulletin of the World Health Organization, 83*, 707–710.

Skansi, S. (2018). *Introduction to Deep Learning: from logical calculus to artificial intelligence.* Springer. doi:https://doi.org/10.1007/978-3-319-73004-2

Summers, R. (2020). *NIH Clinical Center:dataset of 32,000 CT images.* Retrieved from https://www.nih.gov/news-events/news-releases/nih-clinical-center-releases-dataset-32000-ct-images

Szegedy, C., Liu, W., Jia, Y., Sermanet, P., Reed, S., Anguelov, D., & Rabinovich, A. (2015). Going deeper with convolutions. *Proceedings of the IEEE conference on computer vision and pattern recognition*, (pp. 1–9). https://doi.org/10.1109/CVPR.2015.7298594

Wang(d), G., Liu, X., Li, C., Xu, Z., Ruan, J., Zhu, H., & Zhang, S. (2020). A Noise-robust Framework for Automatic Segmentation of COVID-19 Pneumonia Lesions from CT Images_. *IEEE Transactions on Medical Imaging*. https://doi.org/10.1109/TMI.2020.3000314

Wang, L., & Wong, A. (2020). COVID-Net: A Tailored Deep Convolutional Neural Network Design for Detection of COVID-19 Cases from Chest X-Ray Images. *arXiv preprint arXiv:2003.09871*.

Wang, X., Deng, X., Fu, Q., Zhou, Q., Feng, J., Ma, H., & Zheng, C. (2020). A Weakly-supervised Framework for COVID-19 Classification and Lesion Localization from Chest CT. *IEEE Transactions on Medical Imaging*. https://doi.org/10.1109/tmi.2020.2995965

Wani, M. A., Bhat, F. A., Afzal, S., & Khan, A. I. (2020). *Advances in deep learning* (Vol. 57). Springer. https://doi.org/10.1007/978-981-13-6794-6

Weiss, S. R., & Leibowitz, J. L. (2011). Coronavirus pathogenesis. In *Advances in virus research* (Vol. 81, pp. 85–164). Elsevier. https://doi.org/10.1016/B978-0-12-385885-6.00009-2

Williams, T., & Li, R. (2016). Advanced image classification using wavelets and convolutional neural networks. *2016 15th IEEE international conference on machine learning and applications (ICMLA)*, (pp. 233–239). https://doi.org/10.1109/icmla.2016.0046

Wu, J. (2013). Institute of Genomics, Chinese Academy of Science, China National Center for Bioinformation & National Genomics Data Center. *Institute of Genomics, Chinese Academy of Science, China National Center for Bioinformation & National Genomics Data Center*. China. Retrieved from https://bigd.big.ac.cn/ncov/?lang=en

Wu, X., Hui, H., Niu, M., Li, L., Wang, L., He, B., et al. (2020). Deep learning-based multi-view fusion model for screening 2019 novel coronavirus pneumonia: a multicentre study. *European Journal of Radiology*, 109041.

Yang, S., Jiang, L., Cao, Z., Wang, L., Cao, J., Feng, R., & Shan, F. (2020). Deep learning for detecting corona virus disease 2019 (COVID-19) on high-resolution computed tomography: a pilot study. *Annals of Translational Medicine, 8*. https://doi.org/10.21037/atm.2020.03.132

Yang, W., Cao, Q., Qin, L., Wang, X., Cheng, Z., Pan, A., & others. (2020). Clinical characteristics and imaging manifestations of the 2019 novel coronavirus disease (COVID-19): A multi-center study in Wenzhou city, Zhejiang, China. *Journal of Infection*. https://doi.org/10.1016/j.jinf.2020.02.016

Zeiler, M. D., & Fergus, R. (2014). Visualizing and understanding convolutional networks. *European conference on computer vision*, (pp. 818–833). https://doi.org/10.1007/978-3-319-10590-1_53

Zhang, J., Xie, Y., Li, Y., Shen, C., & Xia, Y. (2020). Covid-19 screening on chest x-ray images using deep learning based anomaly detection. *arXiv preprint arXiv:2003.12338*.

Zhu, N., Zhang, D., Wang, W., & others. (n.d.). China Novel Coronavirus Investigating and Research Team. A novel coronavirus from patients with pneumonia in China, 2019 [published January 24, 2020]. *N Engl J Med*. doi:https://doi.org/10.1056/NEJMoa2001017

Zimmerman, D. W., & Zumbo, B. D. (1993). Relative power of the Wilcoxon test, the Friedman test, and repeated-measures ANOVA on ranks. *The Journal of Experimental Education, 62*, 75–86. https://doi.org/10.1080/00220973.1993.9943832